1. Title: The Effect of Transverse Shock Propagation on the Shock-to-Detonation Transition Process for an Insensitive Explosive

2. Authors: Eric K. Anderson, Tariq D. Aslam, Scott I. Jackson
Affiliation: Shock and Detonation Physics Group, Dynamic and Energetic Materials Division, Los Alamos National Laboratory, Los Alamos, NM 87545 USA

3. Corresponding Author's Contact Information:
Eric Anderson
Los Alamos National Laboratory
P.O. Box 1663, MS P952
Los Alamos, NM 87545
USA
Fax: +1 505 667 6372
Email: eanderson@lanl.gov

4. Colloquium Detonations, Explosions, and Supersonic Combustion

5. Paper Length (Method 2): (6200 words max)
900 x 6 + 2.2 x 363 = 6199
6. Word Equivalents:

7. Color Reproduction Charges: None required.

Abstract

The one-dimensional (1D) shock-to-detonation transition process has been studied extensively for PBX 9502, resulting in a good ability to predict the time or distance to detonation over a range of planar input shock pressures. The results are often represented as run distance or time versus input shock pressure on Pop plots. In practice, however, input shocks to explosives are often not 1D. Instead, they may be oblique or non-planar. Here, we present results from a series of experiments in which a PBX 9502 slab was bonded on one side to a PBX 9501 slab. The faster detonation in the PBX 9501 slab drove an oblique shock in the PBX 9502. The result was a two-dimensional (2D) shock structure consisting of a region of delayed reaction, referred to as an initiating layer, immediately adjacent to the PBX 9501/9502 interface, and a transition to detonation further from the interface. The initiating layer thickness varied with the input shock pressure, which was controlled by the thickness of the PBX 9501 layer. The results of seven such tests are presented in run-time vs. input-shock-pressure space and compared to Pop plots generated with data from 1D experiments. Good agreement was observed, with the 2D results showing similar run-times to detonation, but more scatter for a given input shock pressure. The good correlation between the 1D and 2D data suggests the transverse component of the initiating shock does not have a significant effect on the initiation physics.

Keywords

shock, detonation, initiation, transition

1. Introduction

Detonation initiation often occurs by a process in which sensitive booster explosives transmit a shock to a less sensitive main charge. For this reason, shock initiation experiments are an active area of research. Wedge-tests and gas-gun experiments produce accurate measurements of time and distance to detonation in configurations where an explosive is shocked by a planar wave traveling normal to its surface [1–3]. In practice, however, detonations are often not initiated with a one-dimensional (1D) drive, but rather by a shock traveling at some non-zero angle with respect to the surface of the explosive.

The case of a shock traveling parallel to the surface of an explosive produces interesting effects. Such a shock may be generated by placing two explosives with different detonation velocities adjacent to one another, and initiating the pair on a face perpendicular to the shared face. The detonation in the faster explosive outruns the initial detonation in the slower explosive, and drives a shock that is trailed by a detonation in the slower explosive at a speed faster than the detonation velocity of the slower explosive on its own.

This behavior is exhibited by assemblies with an HMX-based explosive slab adjacent to a TATB-based explosive slab, where HMX is the faster explosive. A study of such a configuration was conducted at Los Alamos in 1969 using X-Ray imaging [4]. An image resulting from the study is shown in Fig. 1, where PBX 9404 (an early HMX-based explosive) was used as the sensitive driver explosive on the left, and X0237 (an insensitive explosive consisting of 90% TATB, 5% wax, and 5% Elvax) was on the right. In the figure, a nearly planar driver detonation is visible in the PBX 9404, and a steeply sloped initiating layer is visible in the X0237 adjacent to the PBX 9404. Beyond the initiating layer, a less steeply sloped detonation is visible in the remaining X0237. At the time, this image led some to believe that the initiating layer would widen as the shock structure traveled through the assembly, with eventual failure of detonation in the X0237 [5].

It was more recently shown that, in some cases, the initiating layer does not continue to grow in width as the detonation develops, but rather stabilizes at a finite value. This was observed in an experiment by Matignon et. al [6], where a 50 mm cylinder of T2 (97% TATB, 3% binder) was placed inside a tube of X1 (96% HMX, 4% binder). Of the two explosives, the X1 has the faster detonation velocity. Results indicated a steady detonation front at the center of the T2 cylinder with an initiating layer near the interface with the X1.

Hill and Aslam [7] recently experimentally investigated the case of a 3-mm-thick PBX 9501 (95% HMX, 2.5% Estane, 2.5% BDNPAF) layer adjacent to an 8-mm-thick PBX 9502 (95% TATB, 5% Kel-F 800) layer. Confinement of 304 stainless steel or PMMA was placed on the sides of the assembly. They found that, for this geometry and given adequate run distance, the initiating layer thickness stabilized in the slower PBX 9502. Relating the initiating layer thickness to run-distance in a 1D shock initiation experiment, they used a linear U - u_p relationship to compute the pressure in the initiating layer (U is shock velocity while u_p is particle velocity).

In Anderson et al. [8], the results of five tests to extend the PBX 9501/9502 dual-slab tests to configurations with PBX 9501 thicknesses of 2.5 mm down to 0.5 mm were reported. This test series was conducted with no confinement. Decreasing the thickness of the PBX 9501 layer was found to increase the thickness of the initiating layer until the case of the 1.0 mm PBX 9501, where a transition to detonation did not occur. Further decreasing the thickness of the PBX 9501 layer resulted in similar detonation speeds for both explosives.

In the present work, we build on the experimental results of Anderson et al. [8] to extend the analysis by using a Mie-Grüneisen-Keane equation of state (EOS) to compute shock pressures in the initiating layer. We combine the shock pressure results with the time to detonation as calculated by tracking the progress of an observer riding the shock in the explosive as it travels across the initiating layer. These results are compared to previous layered PBX 9501/9502 [7] and 1D PBX 9502 [2] shock initiation data.

2. Experiments

2.1. Setup

Dual slab tests were conducted [8] using the configuration shown in Fig. 2. For each assembly, a PBX 9502 slab was bonded to a PBX 9501 slab. Explosive dimensions and densities are listed in Table 1. Table 2 lists important properties for the two explosives. The initiating train consisted of a Teledyne RISI Inc. RP-2 detonator, line wave generator, and an 8 mm x 8 mm x 150 mm Composition B booster. Visible in Fig. 2 are ionization wires to measure the phase velocity of the detonation and a streak camera imaging surface to record the detonation front shape at breakout. These measurements typically resolve steady phase velocities to better than 0.010 mm/μs and front curvature features as small as 10 μm.

2.2. Results

Ionization wires were placed on both sides of the explosive assemblies and were measured to within ± 0.5 μm using an optical comparator. Wire positions were combined with time-of-arrival data recorded on an oscilloscope sampling at 5 GS/s with 1 GHz bandwidth. A linear fit to the resulting time-position data was computed, and the slope is reported as the phase velocity D_0 in Table 3. Ionization wire results from the case of the 2.5 mm PBX 9501 slab are shown in Fig. 3.

The streak camera images of the detonation breakout provided a record of the detonation wave shape in time-distance space. Using D_0, time can be converted to distance along the axis of detonation propagation. Sample streak camera images for the cases of 1.5 mm - 2.5 mm thick PBX 9501 layers are shown in Fig. 4. The resulting front shape for the case of the 1.5-mm-thick PBX 9501 layer assembly is shown in Fig. 5. The front shape data can be used to extract the *average* shock deflection angle ϕ and shock normal velocity U_n. U_n is computed by fitting a line to the initiating layer front-shape data, and values for each shot are listed in Table 3 for each assembly. The standard error associated with the fit used to compute U_n is listed following the ± symbols. The shock deflection angle ϕ is computed as $\phi = \arctan\left(\frac{U_n}{D_0}\right)$, and the error associated with ϕ is listed following the ± symbols, calculated from propagation of errors in U_n and D_0.

The PBX 9502 front shape in Fig. 5 has a well-defined change in slope approximately 2.3 mm from the exposed PBX 9501 face. A method was devised [8] to accurately calculate this point by computing a linear fit for each point along the front using the neighboring points within windows 0.16, 0.32, 0.48, 0.64, and 0.80 mm in size. A slope from these fits was then associated with each point along the front, and the location of the maximum change in slope from the 0.16 mm window fits was used to determine the point of transition from initiating layer to detonation. Using this point and the interface with the PBX 9501 slab as boundaries, the thickness of the initiating layer for each assembly was computed and is listed in Table 3. The uncertainty in initiating layer thickness is indicated for each experiment by the ± symbols, and was calculated as the difference between the largest and smallest initiating layer determined by the 0.16-0.80 mm fit windows.

For the case of the assembly with the 0.5-mm-thick PBX 9501 layer, no initiating layer was observed. For this assembly, both explosives were initiated by the booster and detonated with nearly equal velocities. For the 1.0-mm-thick PBX 9501 assembly, the entire PBX 9502 slab exhibited a steeply sloped shock characteristic of an initiating layer. For the assemblies with 1.5–2.5 mm-thick PBX 9501 slabs, front shapes with initiating layers on the order of 1-mm thick were observed. The thickness of the initiating layer decreased with increasing PBX 9501 slab thickness.

3. Analysis of Transverse Initiation Experiments

In this series of experiments, shock pressure was not measured directly. However, using experimentally measured phase velocities and shock angles, a normal velocity in the PBX 9502 initiating layer can be computed. A normal shock analysis that computes jump conditions across a range of shock velocities can then be used to compute the jump conditions for the oblique initiating layer shock.

The normal shock analysis uses the conservation equations for a normal shock

$$\rho_i(-U) = \rho\left(u_p - U\right) \tag{1}$$

$$p_i + \rho_i U^2 = p + \rho\left(u_p - U\right)^2 \tag{2}$$

$$\frac{p_i}{\rho_i} + e_i + \frac{1}{2}U^2 = \frac{p}{\rho} + e + \frac{1}{2}\left(u_p - U\right)^2 \tag{3}$$

where ρ and ρ_i are the downstream and upstream densities, respectively, u_p is the downstream particle velocity in the laboratory frame, U is the shock velocity, p and p_i are the downstream and upstream pressures, and e and e_i are the downstream and upstream specific internal energies. Equations (1)-(3) can be simplified by assuming p_i is small relative to other terms.

An EOS that provides good agreement with experimental data on PBX 9502 is the Mie-Grüneisen

Keane EOS [9], which starts with the following relationship between pressure and density along an isentrope:

$$p_s(\rho) = \frac{K_0' K_0}{K_\infty'^2}\left(\left(\frac{\rho}{\rho_0}\right)^{K_\infty'} - 1\right) - \frac{K_0' - K_\infty'}{K_\infty'} K_0 \ln \frac{\rho}{\rho_0} \tag{4}$$

where p_s is pressure along an isentrope, ρ_0 is a reference density, K_0 is the isentropic bulk modulus at zero pressure, K_0' is the derivative of the isentropic bulk modulus with respect to pressure at zero pressure, and K_∞' is the derivative of the isentropic bulk modulus with respect to pressure at infinite pressure.

Energy along this reference isentrope is determined by integrating $\frac{p}{\rho^2}$, giving

$$e_s(\rho) = \int_{\rho_0}^{\rho} \frac{p_s(\tilde{\rho})}{\tilde{\rho}^2} d\tilde{\rho}. \tag{5}$$

Substituting Eq. (4) into (5) and performing the integration, the expression

$$e_s(\rho) = \frac{K_0\left(-\left(K_0'+1\right)K_\infty'^2(\rho-\rho_0) + K_0'\rho_0\left(\left(\frac{\rho}{\rho_0}\right)^{K_\infty'} - 1\right)\right)}{(K_\infty'-1)K_\infty'^2\rho\rho_0} + \frac{K_0\left((K_\infty'-1)K_\infty'\rho_0\left(K_0'-K_\infty'\right)\ln\frac{\rho}{\rho_0} + K_\infty'^3(\rho-\rho_0)\right)}{(K_\infty'-1)K_\infty'^2\rho\rho_0} \tag{6}$$

is obtained. A hydrodynamic EOS off the isentrope can then be constructed as

$$e(p,\rho) = e_s(\rho) + \frac{p - p_s(\rho)}{\rho\Gamma(\rho)}, \tag{7}$$

where the Grüneisen parameter, Γ, is computed as

$$\Gamma(\rho) = \Gamma_0\left(\frac{\rho_0}{\rho}\right)^q. \tag{8}$$

The Mie-Grüneisen Keane parameters ρ_0, K_0, K_0', K_∞', Γ_0 used for this analysis are given for PBX 9502 in Table 4.

Equations (1), (2), (3), and (7) contain five unknowns: U, u_p, p, ρ, and e. However, the equations can be used to generate a look-up table for four of the unknowns by specifying a single unknown. Downstream density ρ was chosen as the independent variable and was varied from the upstream density ρ_0 to $4\rho_0$ in 1000 steps. The result is a set of tabulated jump conditions for a given shock density, or shock velocity. To extend these results to the oblique initiating layer shock, we simply find normal shock jump conditions corresponding to a normal shock velocity component U_n as defined in Fig. 5. Shock pressures computed using this analysis are listed in Table 3. Results are only shown for the 1.5-2.5–mm-thick PBX 9501 assemblies because a steady initiating layer was not observed in the other assemblies.

4. Comparison to 1D Shock-to-Detonation Transition

Pop plots present the distance or time to detonation as a function of input shock pressure for a given explosive. They are generally used to present data from 1D experiments with a planar input shock. Similarly, for obliquely shocked PBX 9502 in our dual slab experiments, we see the initiating layer varies in thickness as a function of PBX 9501 thickness, which is related to the pressure of the initiating shock. We can present the initiating layer thickness as a function of input shock pressure on a plot similar to a Pop plot, but this would neglect the two-dimensionality of the oblique initiating shock. A more analogous comparison is to consider time to detonation as a function of input shock pressure, as described below.

To compute time to detonation, we consider the time required for an observer riding along the initiating layer and traveling normal to its surface to go from the PBX 9501/9502 interface to the initiating/detonating PBX 9502 boundary. At time $t = 0$ in Fig. 6, the observer is located at the intersection of the shock with the PBX 9501/9502 interface. At a time equal to the run time to detonation, the observer is at the edge of the initiating layer, where the transition to detonation occurs. Shown in the diagram are the normal velocity in the initiating layer U_n and the x and y components of the normal velocity, U_x and U_y. Experimental data provides the shock angle ϕ and phase velocity D_0 from which we compute U_n following a geometric analysis of Fig. 5. Geometric analysis of Fig. 6 allows the x-component of U_n to be computed, and the run time to detonation is then simply the initiating layer thickness divided by U_x. Time-to-detonation values computed using this method are listed in Table 3.

Shock-to-detonation times for the 1.5-2.5 mm-thick PBX 9501 assemblies are shown as a function of shock pressure in Fig. 7, along with the results of Hill and Aslam [7], and lines representing 1D shock-to-detonation transition data from Gustavsen et al. [2]. In the figure, the circular markers represent the results of the 1.5, 2.0, and 2.5 mm layered slab experiments while the solid line represents the fit to 1D data presented in Gustavsen et al. [2]. The dashed lines represent ±20% variation from the fit. Open symbols show the individual 1D data from Gustavsen et al. [2].

Gustavsen et al. [2] computed shock pressures with a linear U-u_p relationship rather than the Mie-Grüneisen Keane EOS utilized in the present study. Therefore, to maintain consistency, we recomputed these pressures using the Mie-Grüneisen Keane EOS with the shock velocities and run times of Gustavsen et al. [2]. These are the results shown in Fig. 7, and the fit to the 1D time to detonation data is

$$\log(t) = 4.31 - 3.62 \log(P). \quad (9)$$

The square markers of Fig. 7 represent four layered PBX 9501/9502 slab tests by Hill and Aslam [7]. These tests were conducted using a geometry identical to that of Fig. 2, but with 3-mm-thick PBX 9501 layers and 4-mm-thick 304 stainless steel or PMMA on both sides of the assemblies. The PBX 9502 densities were also approximately 1% higher than for the 1.5, 2.0, and 2.5 mm PBX 9501 assemblies. The pressures for these tests were also computed using the Mie-Grüneisen Keane EOS.

The square marker with the shortest time to detonation represents the test from Hill and Aslam [7] with PMMA rather than stainless steel on the PBX 9502 side of the assembly. The results of this test fell between those from Anderson et al. [8], which were conducted without confinement. The other three tests from Hill and Aslam [7] were conducted with SS 304 confinement on both sides of the assemblies, and produced lower PBX 9502 shock pressures and longer run-times.

As mentioned, the PBX 9502 density used for the tests [8] represented by the circular markers of Fig. 7 was approximately 1% lower than the normally specified value of 1.890 g/cm^3. The effect of such a change in density generally increases the sensitivity of the explosive, which results in a reduced run-time to detonation for a given input shock pressure. This would be seen in Fig. 7 as a downward shift of the run-time versus shock pressure curve. This effect is difficult to discern for the results presented in Fig. 7, and the varying confinement may have resulted in a competing effect.

Agreement with the 1D run-time vs. pressure curves is generally quite good, with all but two of the tests falling near or within the dashed ±20% lines. The overall trend matches the 1D data quite well, albeit with increased scatter in the data. It should be noted that the 1D results used to generate the fit were taken with lower shock pressures than the results for the transversely initiated PBX 9502.

5. Conclusions

Five assemblies consisting of a PBX 9501 slab bonded to a PBX 9502 slab were detonated at one end and detonation phase velocities and front shapes were measured. In cases with sufficiently thick PBX 9501 layers, the faster detonation in the PBX 9501 drove a shock structure through the PBX 9502 at the speed of the PBX 9501 detonation. The shock structure consisted of an initiating layer, or region of delayed reaction and slow shock normal velocities, immediately adjacent to the PBX 9501. Beyond the initiating layer, an abrupt transition to detonation was observed. The thickness of the initiating layer increased with decreasing PBX 9501 thickness until the case of the 1.0-mm PBX 9501 slab, where initiating layer was observed across the entire 8-mm-thick PBX 9502 slab. For the case of the 0.5-mm-thick PBX 9501 slab, both the PBX 9501 and PBX 9502 detonated with similar velocities and no initiating layer was observed.

An analysis of the experimental results was performed to compute shock pressures in the initiating layer and time to detonation for an observer riding along the shock starting at the PBX 9501/9502 interface. A Mie-Grüneisen Keane equation of state for unreacted PBX 9502 was used to relate measured normal shock velocity and shock pressure. The results for the transversely initiated PBX 9502 showed good agreement with the 1D run-time versus pressure trend, with increased scatter. The good correlation between the 1D and 2D data shows that the transverse component of the initiating shock does not have a significant effect on the initiation physics.

Acknowledgments

This effort was funded by the U.S. Department of Energy Campaign 2: "Dynamic Material Properties." Experiments were assembled and fielded with assistance provided by Sam Vincent and Tim Tucker.

References

[1] J. B. Ramsay, A. Popolato, in: 4th Symposium (Int.) on Detonation, Office of Naval Research, 1965, pp. 233–237.

[2] R. L. Gustavsen, S. A. Sheffield, R. R. Alcon, J. Appl. Phys. 99 (2006).

[3] S. A. Sheffield, R. Engelke, R. R. Alcon, in: Ninth Symposium (Int.) on Detonation, Office of Naval Research, 1989, pp. 39–49.

[4] C. L. Mader (Ed.), LASL Phermex Data Volume III, Los Alamos Series on Dynamic Material Properties, University of California Press, Berkeley, CA, 1980.

[5] W. C. Davis, in: Fourteenth Symposium (Int.) on Detonation, Office of Naval Research, 2010, pp. 1058–1064.

[6] C. Matignon, R. Sorin, O. Bozier, in: Fourteenth Symposium (Int.) on Detonation, Office of Naval Research, 2010, pp. 1182–1190.

[7] L. Hill, T. D. Aslam, in: Seattle, WA, Presented at the Joint SCCM/AIRAPT Conference, Seattle, WA, 2013.

[8] E. K. Anderson, T. D. Aslam, S. I. Jackson, Combustion and Flame (2014) http://dx.doi.org/10.1016/j.combustflame.2013.12.023. In Press.

[9] T. D. Aslam, R. L. Gustavsen, N. L. Sanchez, B. D. Bartram, in: Shock Compression of Condensed Matter, American Institute of Physics, 2011, p. 767.

[10] B. M. Dobratz, P. C. Crawford (Eds.), LLNL Explosives Handbook, Lawrence Livermore National Laboratory, Livermore, CA, 1985.

Tables

Table 1: Measured dimensions in mm and densities in g/cm^3 of assemblies tested. Length and width measured for PBX 9502 slab. * indicates nominal value.

Length	Width	PBX 9502 Thickness	PBX 9502 Density	PBX 9501 Thickness	PBX 9501 Density
149.96	130.02	8.00	1.8719	0.56	1.8354
150.02	129.99	8.00	1.8697	1.14	1.8346
149.96	130.07	8.00	1.8722	1.55	1.8355
150.00	130.00	8.00	1.8704	2.00	1.8327
150.01	130.02	8*	1.8675	2.5*	1.8342

Table 2: Properties of PBX 9501 and PBX 9502 [10].

	Typical Density (g/cm^3)	CJ Detonation Velocity (mm/μs)	Failure Diameter (mm)
PBX 9501	1.830	8.80	1.52
PBX 9502	1.895	7.71	9.00

Table 3: Summary of experimental and computational results.

PBX 9501 Thickness (mm)	PBX 9501 Phase Velocity (mm/μs)	Standard Error (mm/μs)	Initiating Layer ϕ (°)	Initiating Layer U_n (mm/μs)	Initiating Layer Thickness (mm)	Initiating Shock Pressure (GPa)	Time to Detonation (μs)
0.56	7.496	0.0410	none	none	none	N/A	N/A
1.14	8.441	0.0020	53.17-60.86	4.11-5.06	>8	N/A	N/A
1.55	8.638	0.0018	46.37±0.04	5.95±0.004	1.17±0.06	20.9	0.271
2.00	8.696	0.0006	42.82±0.05	6.37±0.005	1.05±0.08	25.6	0.242
2.5	8.731	0.0012	43.67±0.05	6.31±0.005	0.80±0.03	24.9	0.183

Table 4: Mie-Grüneisen Keane EOS parameters for PBX 9502.

ρ_0 (g/cm^3)	K_0 (GPa)	K_0'	K_∞'	Γ_0	q
1.890	6.5	23	4	0.5	1

Figures

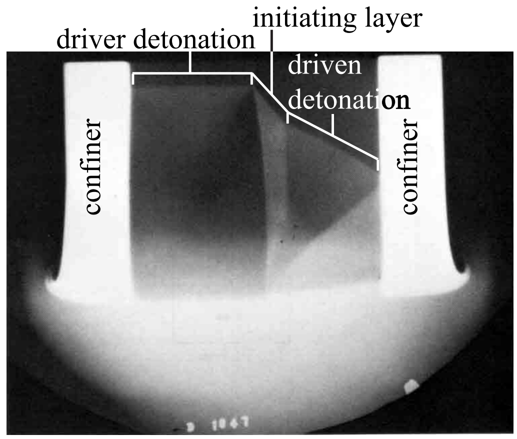

Fig. 1: Flash X-ray image of PBX 9404 shocking X0237 obliquely, with the detonation traveling from the bottom to the top of the image. D. Venable, Shot 1047, LANL 1969 [4].

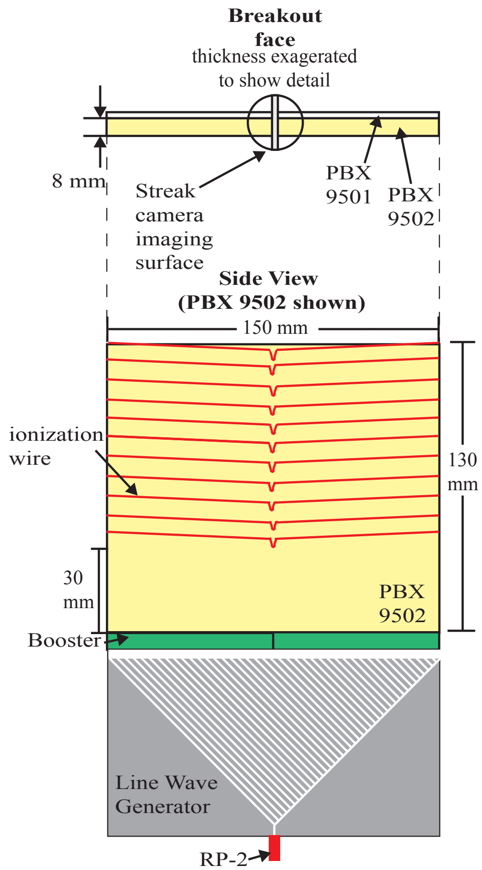

Fig. 2: Diagram of explosive assembly showing key dimensions.

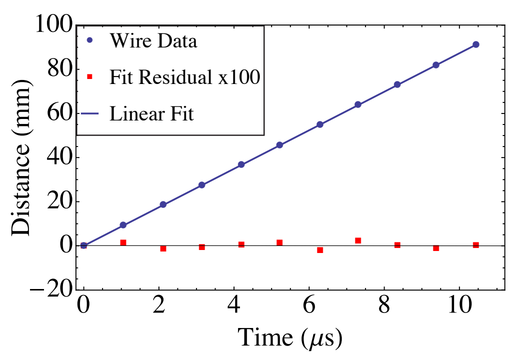

Fig. 3: Ionization wire data from the case of the 2.5 mm PBX 9501 slab. Raw data is shown with circular markers, and the line represents the least-squares fit to the data. The square markers indicate fit residual multiplied by 100.

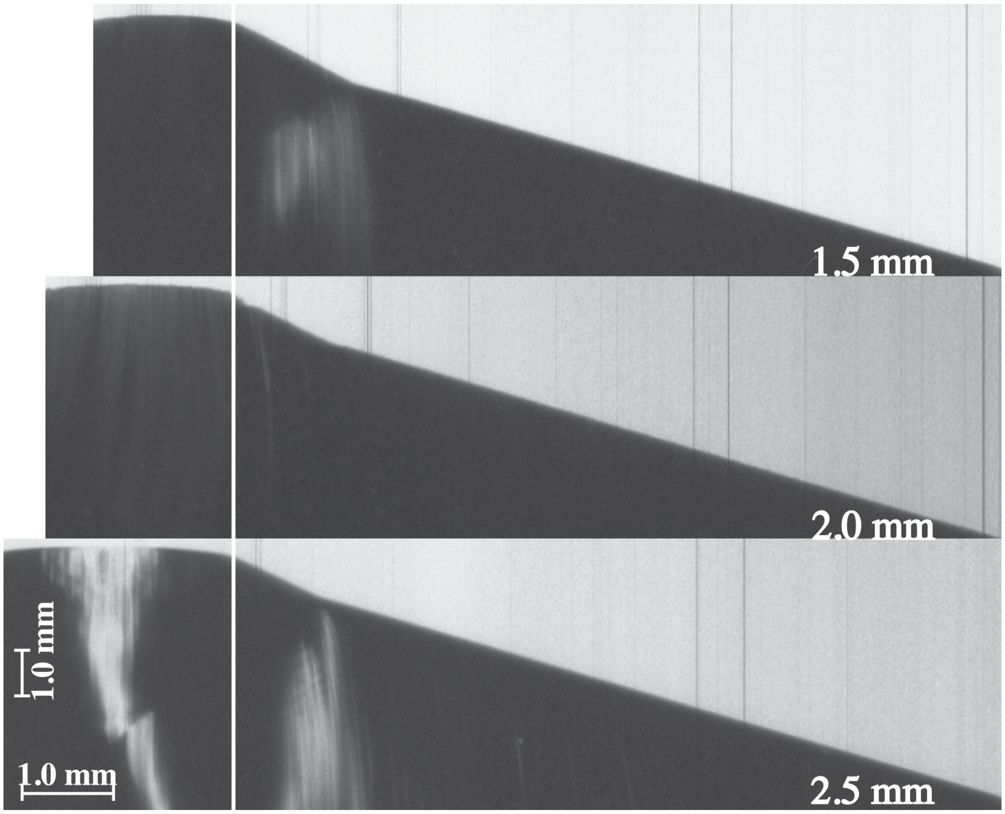

Fig. 4: Front shapes recorded on a streak camera. The thickness of the PBX 9501 is labeled on the lower right corner of each image, and the scaling is shown at the lower left. The vertical line represents the interface between the PBX 9501 (left) and PBX 9502 (right).

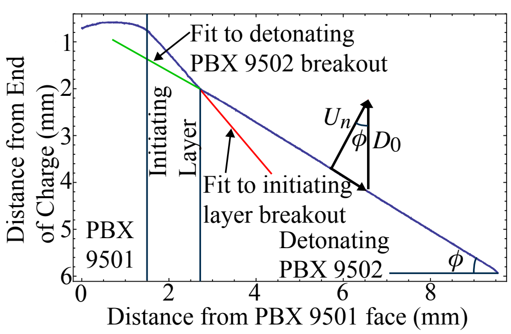

Fig. 5: Front shape for the 1.5-mm-thick PBX 9501 layer assembly. Shock angle and shock normal velocity are labeled on the right, and the intersection used to determine initiating layer thickness is shown on the left.

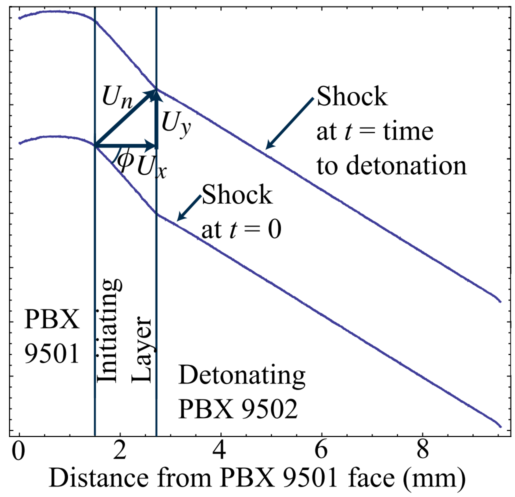

Fig. 6: Geometric analysis used to determine time to detonation.

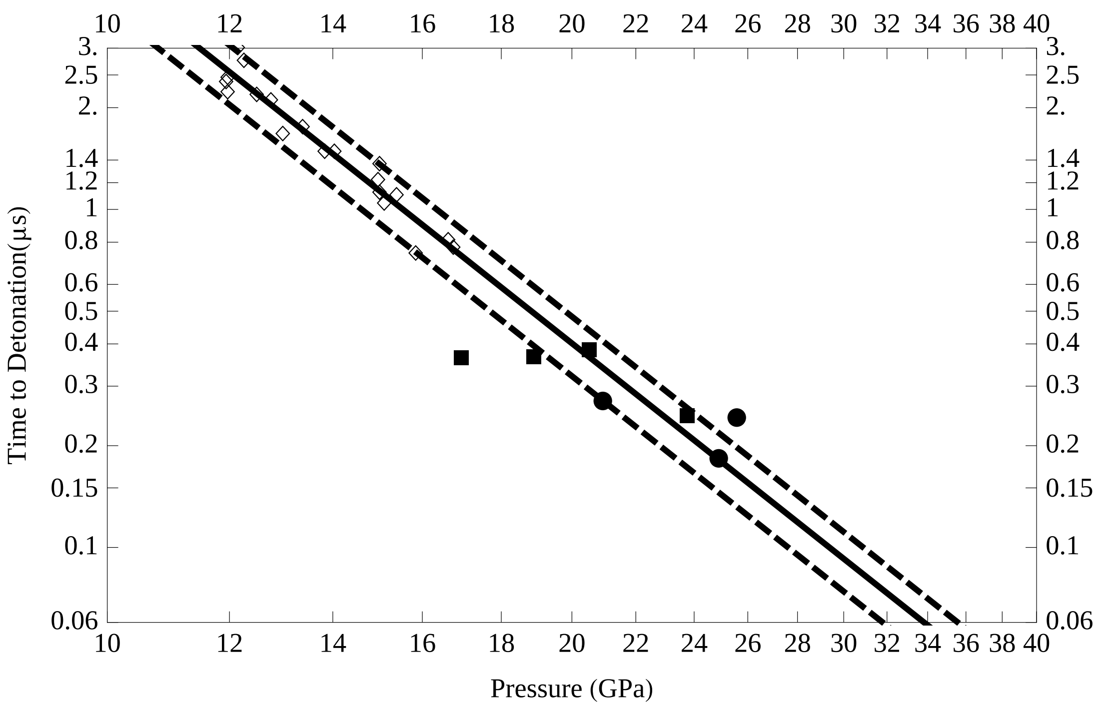

Fig. 7: Time to detonation plotted against input shock pressure. Unconfined PBX 9501/9502 assemblies [8] are represented by the circular markers (●) and SS 304 or PMMA confined PBX 9501/9502 assemblies [7] are represented by square markers (■). The diamond-shaped markers (◇) represent 1D results for PBX 9502 [2], the solid line represents the best fit to their [2] data, and the dashed lines represent a fit uncertainty of ± 20%.

Table Captions

Table 1: Measured dimensions in mm and densities in g/cm^3 of assemblies tested. Length and width measured for PBX 9502 slab. * indicates nominal value.

Table 2: Properties of PBX 9501 and PBX 9502 [10].

Table 3: Summary of experimental and computational results.

Table 4: Mie-Grüneisen Keane EOS parameters for PBX 9502.

Figure Captions

Fig. 1: Flash X-ray image of PBX 9404 shocking X0237 obliquely, with the detonation traveling from the bottom to the top of the image. D. Venable, Shot 1047, LANL 1969 [4].

Fig. 2: Diagram of explosive assembly showing key dimensions.

Fig. 3: Ionization wire data from the case of the 2.5 mm PBX 9501 slab. Raw data is shown with circular markers, and the line represents the least-squares fit to the data. The square markers indicate fit residual multiplied by 100.

Fig. 4: Front shapes recorded on a streak camera. The thickness of the PBX 9501 is labeled on the lower right corner of each image, and the scaling is shown at the lower left. The vertical line represents the interface between the PBX 9501 (left) and PBX 9502 (right).

Fig. 5: Front shape for the 1.5-mm-thick PBX 9501 layer assembly. Shock angle and shock normal velocity are labeled on the right, and the intersection used to determine initiating layer thickness is shown on the left.

Fig. 6: Geometric analysis used to determine time to detonation.

Fig. 7: Time to detonation plotted against input shock pressure. Unconfined PBX 9501/9502 assemblies [8] are represented by the circular markers (●) and SS 304 or PMMA confined PBX 9501/9502 assemblies [7] are represented by square markers (■). The diamond-shaped markers (◇) represent 1D results for PBX 9502 [2], the solid line represents the best fit to their [2] data, and the dashed lines represent a fit uncertainty of ± 20%.